1596–1609 *Nucleic Acids Research, 2010, Vol. 38, No. 5* *Published online 9 December 2009*
doi:10.1093/nar/gkp1145

Gene silencing by cell-penetrating, sequence-selective and nucleic-acid hydrolyzing antibodies

Woo-Ram Lee[1], Ji-Young Jang[2], Jeong-Sun Kim[3], Myung-Hee Kwon[2] and Yong-Sung Kim[1,*]

[1]Department of Molecular Science and Technology, Ajou University, Suwon 443-749, [2]Department of Microbiology, Ajou University School of Medicine, Suwon 442-721 and [3]Department of Chemistry, Chonnam National University, Gwangju, 500-757, Korea

Received September 10, 2009; Revised November 17, 2009; Accepted November 18, 2009

ABSTRACT

Targeting particular mRNAs for degradation is a fascinating approach to achieve gene silencing. Here we describe a new gene silencing tool exploiting a cell-penetrating, nucleic-acid hydrolyzing, single-domain antibody of the light-chain variable domain, 3D8 VL. We generated a synthetic library of 3D8 VL on the yeast surface by randomizing residues located in one of two β-sheets. Using 18-bp single-stranded nucleic acids as target substrates, including the human Her2/neu-targeting sequence, we selected 3D8 VL variants that had ~100–1000-fold higher affinity and ~2–5-fold greater selective hydrolyzing activity for target substrates than for off targets. 3D8 VL variants efficiently penetrated into living cells to be accumulated in the cytosol and selectively decreased the amount of target sequence-carrying mRNAs as well as the proteins encoded by these mRNAs with minimal effects on off-target genes. In particular, one 3D8 VL variant targeting the Her2 sequence showed more efficient downregulation of Her2 expression than a small-interfering RNA targeting the same Her2 sequence, resulting in apoptotic cell death of Her2-overexpressing breast cancer cells. Our results demonstrate that cell-penetrating 3D8 VL variants with sequence-selective, nucleic-acid-hydrolyzing activity can selectively degrade target mRNAs in the cytosol, providing a new gene silencing tool mediated by antibody.

INTRODUCTION

Gene silencing by targeting specific genes for degradation, particularly at the mRNA level, is an invaluable tool for gene function analysis and a powerful therapeutic strategy for human diseases, including cancer and viral infections (1,2). Nucleic-acid based approaches that specifically recognize and hydrolyze particular regions of targeted RNA have been developed for this purpose, including antisense oligonucleotides and interference RNAs (RNAi) (1,2). The RNAi technique is now readily available, in which 21–23 bp double-stranded (ds)-RNAs, so-called small interfering RNAs (siRNA), cause sequence-specific degradation of complementary mRNAs (3,4). Although siRNAs can be directly designed for the target sequence based on Watson–Crick base pairing, their practical application has been limited by several factors, including cellular delivery, nuclease susceptibility and off-target effects (1–4).

Another approach for degrading cytosolic RNAs is the use of protein-based RNases (5) and DNA/RNA-hydrolyzing monoclonal antibodies (mAbs) (6,7), which can penetrate into living cells and degrade cytosolic RNAs. However, these approaches lack high sequence-specificity, leading to significant cytotoxicity (5–7). Although some RNases have been fused with peptides that confer both cell-penetrating and sequence-specific recognition abilities (8,9), these fused RNases cannot be used as a general gene-silencing tool for other genes.

As an alternative approach to conventional techniques, we here describe proof-of-concept for an 'interfering transbody' technology, in which a cell-penetrating antibody (transbody) (10,11) equipped with sequence-specific, nucleic-acid-hydrolyzing activity selectively recognizes and hydrolyzes the target mRNA in the cytosol of living cells, leading to gene silencing (Figure 1A). Recently we reported a sequence-non-specific DNA/RNA-hydrolyzing single-domain antibody of the light-chain variable domain, 3D8 VL (7,12,13), which has cell-penetrating ability. Here, from a yeast surface-displayed 3D8 VL library generated by randomizing potential base-interacting residues, we isolated 3D8 VL

*To whom correspondence should be addressed. Tel: +82 31 219 2662; Fax: +82 31 219 2394; Email: kimys@ajou.ac.kr

The authors wish it to be known that, in their opinion, the first two authors should be regarded as joint First Authors.

variants with target sequence-selective binding and hydrolyzing activity against 18-bp single-stranded (ss)-nucleic acids. The sequence-selective 3D8 VL variants penetrated into living cells and selectively decreased the amounts of the target mRNAs as well as the proteins expressed by these mRNAs, with minimal effects on off-target genes. In particular, a Her2/neu-targeting 3D8 VL variant induced apoptotic cell death of Her2-overexpressing cells by down-regulating Her2 expression after cellular internalization. Our results provide a new gene silencing tool mediated by interfering transbody, which would have potential applications in anti-cancer or anti-viral therapies.

MATERIALS AND METHODS

Materials

All oligonucleotides were synthesized from Integrated DNA technologies (Coralville, IA), unless otherwise specified. Target substrates of 18-bp ss-DNAs and ss-RNAs, G_{18} (5′-GGG GGG GGG GGG GGG GGG-3′ for ss-DNA; $(G_4U)_3G_3$ for ss-RNA) and $Her2_{18}$ (5′-AAT TCC AGT GGC CAT CAA-3′ for ss-DNA; 5′-AAU UCC AGU GGC CAU CAA-3′ for ss-RNA), were synthesized with or without 5′-biotinylation (12,13). Off-target 18 bp ss-DNAs with contiguous stretches of single nucleobases, such as T_{18}, C_{18} and A_{18}, or random sequences N_{18} (N = A/T/G/C) were also synthesized with or without 5′-biotinylation. An off-target substrate of 18-bp ss-RNA N_{18} (N = A/U/G/C) was synthesized as above. To construct enhanced green fluorescent protein (EGFP) (the GFP carries two mutations of Phe64Leu and Ser65Thr) reporter plasmid, the target sequence of G_{18} and $Her2_{18}$ was placed between the ATG start codon and EGFP coding sequence in the pEGFP-N1 plasmid (Clontech), resulting in pG_{18}-EGFP and $pHer2_{18}$-EGFP, respectively. The full-length Her2 cDNA (NCBI accession no. M11730) was subcloned into pcDNA3.1(+) with NheI and BamHI sites, resulting in pcDNA3-Her2. $Her2_{18}$-siRNA, which has the sequence 5′- AAU UCC AGU GGC CAU CAA AdTdT-3′, was synthesized at Bioneer Co. (Daejeon, Korea). All other reagents were analytical grade, the details of which are provided in the Supplementary Data.

3D8 VL library construction and screening

The gene encoding 3D8 VL derivative 4M, which has four mutations of Q42R, Y49H, W50R and H94A, compared with 3D8 VL wild-type (WT) (NCBI accession no. AAF79129) (12,13), was subcloned in-frame into the yeast surface display plasmid, pCTCON (14). Using 3D8 VL 4M as a template (Supplementary Figure S1), the 3D8 VL library was generated by serial overlapping PCRs to reconstitute full-size products using five partially overlapping oligonucleotides and two flanking oligonucleotides, which were designed to randomize targeted mutation residues at the in C-, C′-, F-strands with the NNB codon. Library construction (Supplementary Figure S1) and library screening against biotinylated-target ss-DNAs (Supplementary Figure S2) were conducted using previously described protocols (14) (also see Supplementary Data for details).

Protein preparation and biochemical analyses

3D8 VL WT and HW1 scFv were prepared from the supernatant of bacterial culture, as essentially described previously (12,13,15). After genes encoding 3D8 VL variants, including 4 M, were subcloned from the yeast surface display vector into in frame the bacterial cytosolic expression plasmid of pETdwHis using NheI/BamHI sites (15), they were expressed in *Escherichia coli* BL21 (DE3). While 4 M expressed solubly in the cytosol of *E. coli* was purified using its C-terminus 6 × His tag (12,13), isolated 3D8 VL variants expressed dominantly in insoluble form of inclusion body were refolded and purified as described previously (16). The yield of purified protein was ~2–3 mg out of 1-l flask culture. Protein concentrations were determined using the Bio-Rad protein assay kit. Biochemical analyses of 3D8 VLs, such as DNA- and RNA-hydrolyzing assays on agarose gels (7,13,17) and surface plasmon resonance (SPR) analysis (12,13) were described previously, the details of which are provided in the figure legends and Supplementary Data.

Sequence-specific nucleic-acid-hydrolyzing assays

Sequence-specific ss-DNA and ss-RNA-hydrolyzing kinetic assays of 3D8 VL WT and its variants were carried out by fluorescence resonance energy transfer (FRET)-based cleavage assay using 18-bp target and off-target substrates, which were double-labeled with a 6-carboxyfluoroscein (FAM^{TM}) at the 5′-terminus and a black-hole quencher ($BHQ^{®}$-1) at the 3′-terminus (Integrated DNA Technologies) (7,18). For ss-DNA FRET substrates, the following substrates were used: A_{18}, 5′-FAM-AAA AAA AAA AAA AAA AAA-BHQ-1-3′; T_{18}, 5′-FAM-TTT TTT TTT TTT TTT TTT-BHQ-1-3′; C_{18}, 5′-FAM-CCC CCC CCC CCC CCC CCC-BHQ-1-3′; $(G_4T)_3G_3$, 5′-FAM-GGG GTG GGG TGG GGT GGG-BHQ-1-3′; $Her2_{18}$, 5′-FAM-AAT TCC AGT GGC CAT CAA-BHQ-1-3′; N_{18}, 5′-FAM-NNN NNN NNN NNN NNN NNN-BHQ-1-3′ (N = A/T/G/C). For ss-RNA FRET substrates, the following two substrates were used: $Her2_{18}$, 5′-FAM-AAU UCC AGU GGC CAU CAA-BHQ-1-3′; N_{18}, 5′-FAM-NNN NNN NNN NNN NNN NNN-BHQ-1-3′ (N = A/U/G/C). FRET reactions were initiated at 37°C in 96-well Greiner black plate (Sigma-Aldrich) by adding 100 µl of 3D8 VLs (final 100 nM) to 100 µl of samples containing various concentrations of dual-labeled substrates (16 nM–2 µM) in TBS buffer with 2 mM $MgCl_2$ for ss-DNAs or without 2 mM $MgCl_2$ for ss-RNAs. Increase of fluorescence intensity due to the DNA/RNA hydrolysis was immediately measured by excitation at 480 and emission at 525 nm for 30 min at 30 s interval in a fluorescence microplate reader (Molecular Devices). Fluorescence did not significantly increase over time when 10 µM of the dual-labeled oligonucleotides were incubated in reactions without 3D8 VLs. The raw fluorescence data were corrected for background signal determined in the absence of proteins and then scaled so that all the initial values were the same

fluorescence arbitrary value, 0. Arbitrary fluorescence value was converted into substrate concentration using the standard curve, in which fluorescence intensity changes were plotted as a function of substrate concentrations that were completely digested by DNase I for ss-DNA substrates and bovine pancreatic RNase A (Invitrogen) for ss-RNA substrates (18). Then initial rate constants (V) at each substrate concentration were determined by linear regression over the initial linear regions (between 0 and 500 s) of the normalized data using Softmax® pro software (Molecular Devices). The apparent enzymatic kinetic parameters, K_m and V_{max}, were determined by fitting the initial rate constants (V) versus substrate concentrations (S) into the Michaelis–Menten equation $[V = (V_{max}[S])/(K_m + [S])]$ and Lineweaver–Burk equation using Sigmaplot 2002 software (SPSS Inc.) (12,18). All experiments were performed in triplicate and the results are expressed as mean ± standard deviation (SD). Significant difference was determined using two-tailed Student's t-test versus the control N_{18} substrate on Excel software (Microsoft Inc.). A P-value of < 0.01 was taken as statistically significant.

Cell penetration

Human cervical carcinoma HeLa, breast carcinoma SK-BR-3 and MDA-MB-231 cells were from American Type Culture Collection (ATCC, Manassas, VA) and cultured in DMEM (Dulbecco's Modified Eagle Medium) supplemented with 10% (v/v) fetal bovine serum, 100 units/ml penicillin, and 100 μg/ml streptomycin (Invitrogen) in a humidified 5% CO_2/95% air atmosphere at 37°C (7,15,19). All of the cell lines were routinely screened for Mycoplasma contamination. Cell penetration experiments and subsequent various analyses were performed as described previously (7,12,15). Cells were seeded at a density of $\sim 5 \times 10^5$ cells/well in 6-well plate (for flow cytometry, RT–PCR, western blotting, and cell viability assays) or $\sim 5 \times 10^4$ cells/well in 24-well plate over glass coverslips (for confocal microscopy) the day before use, and pre-incubated in serum-free DMEM for 30 min at 37°C prior to the treatment of proteins and/or reagents. Then the cells were incubated with 3D8 VLs (each 10 μM) for 2 h at 37°C with or without pre-treatment with 100 IU/ml soluble heparin, chloropromazine (10 μg/ml), methyl-β-cyclodextrin (5 mM) and cytochalasin D (1 μg/ml) for 30 min at 37°C, washed and then further incubated for the indicated periods prior to subjecting to various analyses, as specified in figure legends. Cell viability was analyzed using a colorimetric MTT (3-(4,5-dimethylthiazol-2-yl)-2,5-diphenyltetrazolium bromide)-based cell growth determination kit (Sigma) (7,15,19). The percentage of apoptotic cells was quantified by flow cytometry after fluorescent staining with Annexin-V-FITC and propidium iodide (PI) (19).

Cell transfection

All transfections were performed using Lipofectamine 2000 (Invitrogen Inc.) with plasmid DNA (each 0.5 μg) or $Her2_{18}$-siRNA (500 nM) following the manufacturer's instructions (7). For HeLa cells transfected with plasmid of pEGFP-N1, pG_{18}-EGFP, or pcDNA3-Her2, the cells were treated for 2 h at 37°C with 3D8 VLs (10 μM) after 12 or 24 h post-transfection, washed and then further incubated for the indicated periods prior to subjecting to various analyses. In experiment with SK-BR-3 cells, the cells grown ~50% confluency ($\sim 5 \times 10^5$ cells in 6-well plates) were transfected with $Her2_{18}$-siRNA as above, prior to subjecting to various analyses.

Confocal fluorescence microscopy

Confocal fluorescence microscopic analyses of the cells were performed as described previously (7,15). Briefly, the cells were washed twice with cold PBS, fixed with 2% paraformaldehyde in PBS for 10 min at 25°C, and then permeabilized with Perm-buffer (1% BSA, 0.1% saponine, 0.1% sodium azide in PBS) for 10 min at 25°C. For staining of internalized 3D8 VLs, the cells were blocked with 2% BSA in PBS for 1 h, incubated with rabbit anti-3D8 polyclonal antibodies (7), followed by TRITC-anti-rabbit IgG. Nucleus was stained with DAPI (4′,6-diamidino-2-phenylindole dihydrochloride) (Vector Labs) during the last 10 min of incubation at 25°C. Cells on coverslip were mounted in Vectashield anti-fade mounting medium (Vector Labs), and observed with Zeiss LSM 510 laser confocal microscope and analyzed with Carl Zeiss LSM Immage software.

Flow cytometry

For the quantification of EGFP expression in HeLa cells treated as above, the suspended cells with trypsin were washed twice with 1 ml ice-cold PBS and then directly subjected to flow cytometry on a Becton Dickinson FACSCalibur™ (7,15). For the cells transfected with EGFP and/or treated with 3D8 VLs (10 μM) for cellular internalization as described above, the suspended cells with trypsin were treated once more with 0.1% trypsin for 3 min at 37°C to wash off the surface bound proteins (7). After washings with ice-cold PBS once, the cells were fixed and permeabilized as the procedures described in above 'confocal fluorescence microscopy'. The cells were washed with ice-cold PBS twice, labeled with rabbit anti-3D8 polyclonal antibodies followed by TRITC-anti-rabbit, and then analyzed using the flow cytometry. In experiment with the SK-BR-3 cells transfected with $Her2_{18}$-siRNA or exposed to 3D8 VLs as above, cell-surface expression levels of Her2 were monitored by immunofluorescent labeling of rabbit anti-Her2 mAb (1 h on ice) and then goat FITC-labeled anti-rabbit IgG (1 h on ice) (7,15). For each test, $\sim 1 \times 10^4$ cells were analyzed.

Reverse transcription (RT) PCR

To monitor mRNA levels in cells, semi-quantitative RT–PCR was performed following the standard procedures (7,20). Total cellular RNA was extracted from specified cells, using the Trizol (Gibco Invitrogen), according to the manufacture's instruction. Aliquots (~1 μg) of total RNA were used for first strand complimentary DNA (cDNA) synthesis using PreMix cDNA synthesis kit

(Bioneer, Korea) and oligo dT primer (7). The synthesized cDNA was then diluted and used as a template to amplify transcripts specific for 3D8 VLs, EGFP, Her2, and/or β-actin by PCR with the same number of cycles (30 cycles) (7). The endogenous gene, β-actin, was served to normalize the total amount of mRNA used in each sample (20). The PCR products were then applied to 1% agarose gel electrophoresis followed by ethidium bromide staining.

Western blotting

Western blotting for cell lysates treated as specified in figure legends was performed following the standard procedure, using primary antibodies specific for target molecules (7,15,19). The appropriate secondary IgG conjugated to horse radish peroxidase (Zymed Laboratories) was used for developing by chemiluminescence (Amersham Pharmacia Biotech).

RESULTS

3D8 VL library design and construction

3D8 VL WT possess intrinsic DNA/RNA-hydrolyzing activity without sequence specificity in the presence of a divalent metal ion, including Mg^{2+} and Co^{2+} (12,13,17). Although the structure of the complex between 3D8 VL WT and DNA/RNA is currently unavailable, the recently resolved 3D8 VL WT structure complexed with a phosphate mimetics and Co^{2+} (17) suggests that the residues of Leu33, Tyr49, Trp50, Lys89 and Ser91 are the putative DNA/RNA-hydrolyzing catalytic site. These residues are located in the upper part on one of two β-sheets (Figure 1B), indicating that 3D8 VL might interact with DNA/RNA using the groove formed by the three-stranded β-sheet (C-, C′- and F-strands). The efficient DNA/RNA-hydrolyzing activity of the 3D8 VL WT derivative 4M (Figure 2A and B), which has four substitutions of Q42R, Y49H, W50R and H94A in the groove (Supplementary Figure S3) (13,17), supported the rationale of randomizing residues on the C′-, C- and F-strands to isolate DNA/RNA sequence-specific 3D8 VL variants.

We constructed a yeast surface-displayed 3D8 VL library on the template of 4M by performing successive overlapping PCR mutagenesis, using partially overlapping oligonucleotides designed to introduce random mutations with a degenerate codon NNB at the 15 targeted residues of the C- (35–39 residues), C′- (44–48 residues) and F-strands (84–88 residues) (Figure 1C and Supplementary Figure S1). The NNB codon encodes all 20 amino acids with a reduced stop codon frequency (2.1%) (21). The constructed 3D8 VL library showed the diversity of $\sim 8 \times 10^7$, which sparsely sampled the theoretical sequence space ($> 3 \times 10^{19}$). The initial library with random mutations with 20 possible amino acids at the targeted regions was expressed well on the yeast cell surface (Supplementary Figure S1).

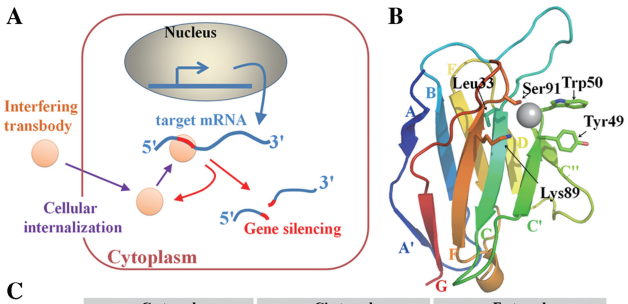

Figure 1. (**A**) Schematic diagrams showing the concept of the interfering transbody. Cell-penetrating antibody (transbody) equipped with sequence-specific nucleic-acid-hydrolyzing activity penetrates into the cytosol of living cells and preferentially recognizes and hydrolyzes the target mRNA, leading to target gene silencing. (**B**) Structural characteristics of 3D8 VL. Three-dimensional structure of the complex between 3D8 VL WT and Co^{2+} (gray ball) (PDB code 3BD5) (17). The putative catalytic residues are highlighted and described in detail in the text. Each β-strand is indicated by a different color code. (**C**) 3D8 VL library generation scheme. The library was generated by randomizing 15 putative nucleic-acid binding residues in the groove composed of the C- (35–39 residues), C′- (44–48 residues) and F-strands (84–88 residues) with a degenerate codon of NNB (N = A/T/G/C, B = C/G/T) based on 3D8 VL 4M as a template (Supplementary Figure S1). Numbering is according to the Kabat definition (12). Amino acids and nucleotide bases are indicated in single-letter code according to IUPAC.

Isolation of 3D8 VL variants against target 18-bp ss-DNA substrates

For model target substrates, we used two 18-bp ss-DNA substrates, contiguous guanine nucleobase (G_{18}) and the Her2/neu-targeting sequence ($Her2_{18}$). The $Her2_{18}$ sequence, corresponding to positions 2391–2408 of the Her2/neu gene, was designed according to an algorithm to search siRNA target sequences (22). The oncogene Her2 is widely overexpressed in many human epithelial tumors, making it an attractive target for anti-cancer agents (22,23). The ss-DNA was employed as a substrate rather than ss-RNA because ss-RNA is highly sensitive to self-hydrolysis. Using two rounds of magnetic activated cell sorting (MACS) followed by four rounds of fluorescence activated cell sorting (FACS) with a high salt (300 mM NaCl) containing buffer and off-target substrates as competitors to counterselect against non-specific binders, six clones against G_{18} and five against $Her2_{18}$ were isolated and designated 4MG1-6 and 4MH1-5, respectively (Supplementary Figures S2 and S3). The isolated 3D8 VL variants contained 5–15 substitutions out of the 15 targeted residues (Supplementary Figure S3).

Biochemical characterization of isolated 3D8 VL variants

All of the isolated variants were subcloned in-frame into a bacterial cytoplasmic expression plasmid. While 3D8 VL WT and 4M were expressed solubly in *E. coli* (12,13), all of the isolated 3D8 VL variants were expressed dominantly in insoluble form of inclusion body. Thus they were refolded and purified with > 90% purity, as shown in SDS–PAGE analyses (Supplementary Figure

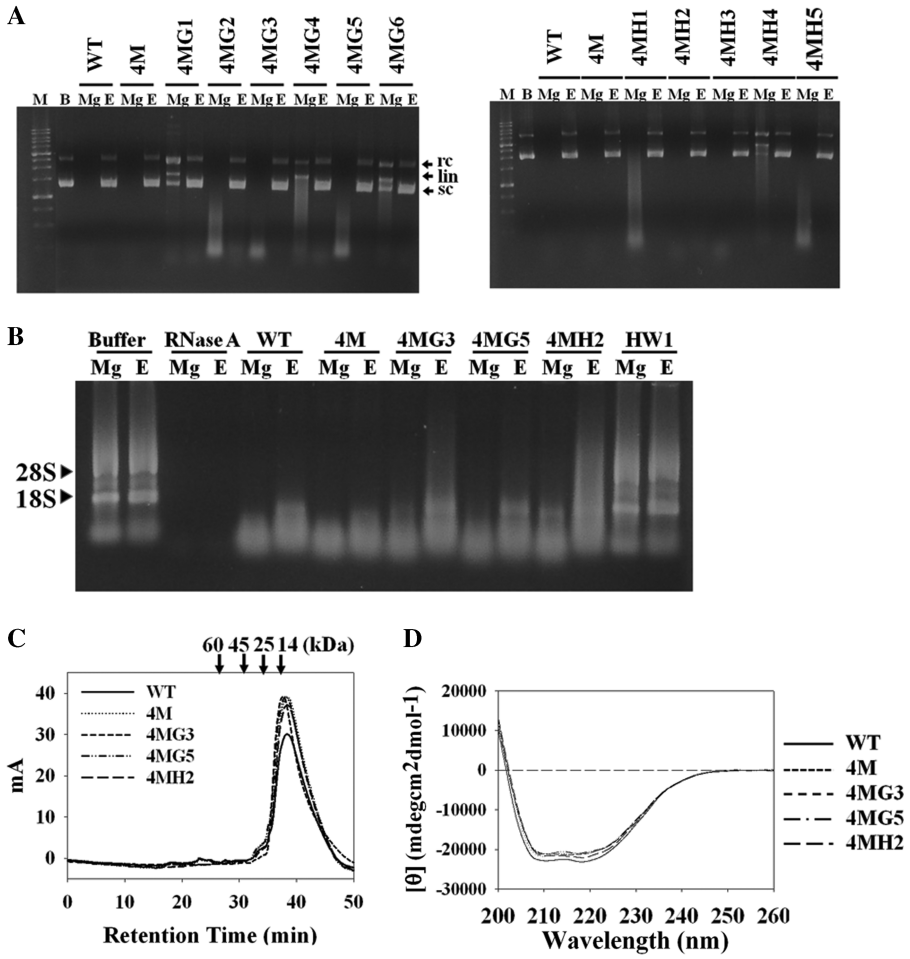

Figure 2. Biochemical characterization of representative 3D8 VL variants selected against ss-DNA G_{18} (4MG3 and 4MG5) and $Her2_{18}$ ss-DNA (4MH2), compared with 3D8 VL WT and 4M. (**A**) DNA hydrolyzing activity analyses of primarily isolated 3D8 VLs selected against ss-DNA G_{18} (4MG1-4MG6) and $Her2_{18}$ ss-DNA (4MH1-4MH5) by agarose gel electrophoresis, compared with 3D8 VL WT and 4 M. The supercoiled plasmid of pUC19 (2.2 nM) was incubated with 3D8 VLs (5 μM) for 1 h at 37°C in the TBS buffer, pH 7.4, containing 2 mM $MgCl_2$ (indicated as 'Mg') or 50 mM EDTA (indicated as 'E'). The reaction mixtures were analyzed by electrophoresis on 0.7% agarose gels, and then stained with ethidium bromide. The arrows indicate supercoiled (*sc*), linear (*lin*) and relaxed circular (*rc*) DNAs. The samples incubated with only buffer alone and molecular mass markers were designated as 'B' and 'M', respectively. (**B**) RNA-hydrolyzing activity of 3D8 VLs, including WT, 4M, G_{18}-selective 4MG3 and 4MG5, and $Her2_{18}$-selective 4MH2. Total cellular RNA (1 μg) extracted from HeLa cells were incubated at 37°C for 2 h in TBS buffer, pH 7.4, containing 2 mM $MgCl_2$ (indicated as 'Mg') or 50 mM EDTA (indicated as 'E') with 3D8 VLs (0.1 μM), RNase A (1 U), irrelevant HW1 scFv protein (0.1 μM) as a negative control prior to gel electrophoresis. The bands corresponding to rRNAs of 28S and 18S are indicated. (**C**) SEC elution profiles of representative 3D8 VLs (~12 kDa). Each protein (20 μM ≈ 260 μg/ml in TBS, pH7.4) indicated in different lines was injected and chromatograms were obtained by absorbance at 280 nm. Arrows indicate the elution positions of mass standard markers (Sigma) [BSA (66 kDa), ovalbumin (45 kDa), chymotrypsinogen A (25 kDa), ribonuclease A (13.7 kDa)]. (**D**) Far-UV CD spectra of representative 3D8 VLs (100 μg/ml in TBS, pH7.4) to monitor the secondary structure are shown.

S4). First, we investigated whether the isolated 3D8 VL variants maintained DNA-hydrolyzing catalytic activity by agarose gel electrophoresis using the supercoiled plasmid of pUC19 as a substrate. Most of the variants efficiently hydrolyzed the substrate in the presence of Mg^{2+}, but not EDTA, demonstrating that they retain DNA-hydrolyzing activity in a Mg^{2+}-dependent manner (Figure 2A), similar to the parents of 3D8 VL WT and 4M (12,13). Among them, we focused further investigation on 4MG3 and 4MG5 isolated against G_{18} as well as 4MH2 isolated against $Her2_{18}$, which showed the most efficient DNA-hydrolyzing activities.

The chosen 3D8 VL variants, including 3D8 VL WT and 4 M, also efficiently hydrolyzed total cellular RNAs extracted from HeLa cells even in the presence of EDTA (Figure 2B), demonstrating that 3D8 VLs possess RNase activity without requirement of divalent metal ions, like RNase A (24). However, an irrelevant HW1 scFv (15) purified from bacterial cells using the same procedure with that of 3D8 VLs did not show the RNA-hydrolyzing activity. This demonstrated that the RNA-hydrolyzing activity of 3D8 VLs was their intrinsic property, but not due to co-purified bacterial nucleases. Taken altogether, the 3D8 VLs have both DNase and RNase activity *in vitro*, like 3D8 scFv (7,12,13).

Size exclusion chromatography (SEC) analyses demonstrated that 3D8 VLs (20 μM ≈ 260 μg/ml) were eluted as single peaks that correspond to an apparent

Table 1. Kinetic binding parameters for the interactions of 3D8 VLs with target and off-target 18-bp ss-DNAs or ss-RNAs, which were monitored by SPR[a]

3D8 VLs	Kinetic parameters	ss-DNA substrates (ss-RNA substrates)[b]					
		A_{18}	T_{18}	C_{18}	G_{18}[ss-RNA $(G_4U)_3G_3$][c]	$Her2_{18}$(ss-RNA)	N_{18}(ss-RNA)
WT	k_{on} ($M^{-1}s^{-1}$) ($\times 10^3$)	0.13 ± 0.04	0.67 ± 0.02	0.78 ± 0.04	0.71 ± 0.01 (0.39 ± 0.02)	1.63 ± 0.30 (0.31 ± 0.02)	0.41 ± 0.03 (0.56 ± 0.02)
	k_{off} (s^{-1}) ($\times 10^{-3}$)	3.24 ± 0.21	6.82 ± 0.13	9.73 ± 0.88	8.26 ± 0.62 (6.27 ± 0.15)	35.2 ± 2.3 (5.39 ± 0.24)	15.4 ± 2.7 (19.3 ± 1.3)
	K_D (M) ($\times 10^{-7}$)	239 ± 13	102 ± 15	126 ± 13	116 ± 15 (159 ± 12)	215 ± 5.3 (174 ± 15)	375 ± 4.2 (344 ± 16)
4M	k_{on} ($M^{-1}s^{-1}$) ($\times 10^3$)	0.60 ± 0.02	3.95 ± 0.21	5.81 ± 0.25	0.49 ± 0.13 (0.54 ± 0.09)	0.24 ± 0.02 (0.14 ± 0.01)	0.96 ± 0.02 (0.49 ± 0.13)
	k_{off} (s^{-1}) ($\times 10^{-3}$)	7.32 ± 0.70	5.80 ± 0.09	5.88 ± 0.71	5.18 ± 0.10 (5.63 ± 0.45)	5.49 ± 0.47 (3.45 ± 0.98)	10.3 ± 1.8 (6.04 ± 0.28)
	K_D (M) ($\times 10^{-7}$)	122 ± 12	14.7 ± 1.6	10.1 ± 1.6	105 ± 23 (104 ± 19)	233 ± 2.7 (252 ± 19)	107 ± 3.5 (123 ± 27)
4MG3	k_{on} ($M^{-1}s^{-1}$) ($\times 10^3$)	0.14 ± 0.03	0.25 ± 0.02	3.07 ± 0.32	1.17 ± 0.3 (1.11 ± 0.08)	0.24 ± 0.04 (0.15 ± 0.02)	0.38 ± 0.02 (0.25 ± 0.03)
	k_{off} (s^{-1}) ($\times 10^{-3}$)	5.24 ± 0.95	2.80 ± 0.19	3.53 ± 0.41	0.09 ± 0.01 (0.08 ± 0.01)	7.55 ± 0.89 (6.80 ± 0.55)	9.37 ± 0.97 (4.26 ± 0.36)
	K_D (M) ($\times 10^{-7}$)	371 ± 28	112 ± 22	115 ± 14	0.76 ± 0.04 (0.72 ± 0.05)	313 ± 24 (441 ± 23)	249 ± 31 (171 ± 12)
4MG5	k_{on} ($M^{-1}s^{-1}$) ($\times 10^3$)	0.26 ± 0.02	0.89 ± 0.04	0.51 ± 0.03	9.02 ± 0.77 (8.18 ± 0.08)	0.45 ± 0.05 (0.56 ± 0.07)	0.13 ± 0.03 (0.16 ± 0.03)
	k_{off} (s^{-1}) ($\times 10^{-3}$)	7.92 ± 0.24	3.13 ± 0.12	1.92 ± 0.11	0.84 ± 0.05 (0.72 ± 0.04)	5.32 ± 0.82 (7.20 ± 0.31)	7.25 ± 0.87 (9.43 ± 0.22)
	K_D (M) ($\times 10^{-7}$)	303 ± 19	35.0 ± 3.6	37.7 ± 2.9	0.93 ± 0.03 (0.88 ± 0.07)	118 ± 29 (129 ± 28)	557 ± 54 (590 ± 22)
4MH2	k_{on} ($M^{-1}s^{-1}$) ($\times 10^3$)	0.13 ± 0.01	0.25 ± 0.05	0.43 ± 0.03	0.42 ± 0.07 (0.23 ± 0.01)	4.41 ± 0.13 (2.45 ± 0.10)	0.17 ± 0.01 (0.18 ± 0.02)
	k_{off} (s^{-1}) ($\times 10^{-3}$)	2.54 ± 0.21	2.51 ± 0.61	4.31 ± 0.87	4.53 ± 0.82 (3.22 ± 0.17)	0.94 ± 0.07 (0.38 ± 0.02)	7.20 ± 0.66 (5.44 ± 0.90)
	K_D (M) ($\times 10^{-7}$)	194 ± 21	103 ± 17	100 ± 22	107 ± 3.4 (143 ± 11)	2.13 ± 0.13 (1.47 ± 0.27)	427 ± 29 (308 ± 21)

[a]Each value represents the mean ± SD of two independent experiments. In each experiment, at least five data sets were used in the determination of the kinetic constants.
[b]The values for ss-RNA substrates, G_{18}, $Her2_{18}$ and N_{18}, were presented in the parenthesis.
[c]Due to the difficulty in synthesizing 5′-biotinylated ss-RNA G_{18}, ss-RNA $(G_4U)_3G_3$ was used as the G_{18} substrate.

molecular mass of each protein, demonstrating that they are existing in monomeric form in solution at concentrations higher than used in DNA- and RNA-hydrolyzing assays (Figure 2C). This result indicates that 3D8 VLs hydrolyze both DNA and RNA in monomeric form. Secondary structures of the 3D8 VL variants, 4MG3, 4MG5 and 4MH2, determined by far-UV circular dichroism (CD) spectroscopy exhibited very similar spectra to those of 3D8 VL WT and 4M, exhibiting a negative maximum of mean residue ellipticity ~217 nm (Figure 2D), which is typical for the immunoglobulin fold (12). This data suggested that the extensive mutations incorporated into the inner β-strands of the 3D8 VL variants did not significantly affect the unique secondary structure.

Selected 3D8 VL variants preferentially bind to hydrolyze target substrates

The specificity and affinity of the selected 3D8 VLs for their respective target ss-DNA/RNA (G_{18} and $Her2_{18}$) and off-targets (A_{18}, T_{18}, C_{18} and N_{18}) were evaluated using SPR technique (13). The kinetic binding parameters are summarized in Table 1. 3D8 VL WT and 4M exhibited indistinguishable binding affinities ($K_D \approx 10^{-5}$ M) for all tested ss-DNA/RNA substrates (12,13), except for the preferential bindings ($K_D \approx 10^{-6}$ M) of 4M and 4MG5 for ss-DNA T_{18} and C_{18} substrates. In contrast, the 3D8 VL variants displayed ~100–1000-fold tighter binding ($K_D \approx 10^{-8}$ M of 4MG3 and 4MG5 against ss-DNA/RNA G_{18}; $K_D \approx 10^{-7}$ M of 4MH2 against ss-DNA/RNA $Her2_{18}$) to target substrates than to off-targets ($K_D \approx 10^{-5}$ M), which was mainly due to the decreased dissociation rate constants (k_{off}) of the target substrates (Table 1). This result indicated that, even though 18-bp ss-DNAs were used as screening probes, the selected 3D8 VL variants maintained preferential binding specificity for the target substrates with the same sequences in ss-RNA form.

We next determined the target sequence-specific hydrolyzing activity of 3D8 VL variants by using a FRET-based cleavage assay with 18-bp target and off-target ss-DNAs as substrates, which were double-labeled with a fluorophore (FAM) at 5′-terminus and its quencher (BHQ®-1) at 3′-terminus (Figure 3) (7,18). The substrate-hydrolyzing can be monitored by following the fluorescence intensity increase caused by the 6-FAM release from its quencher BHQ®-1 due to the hydrolysis (7,18). The reaction velocity of 3D8 VLs exhibited saturation

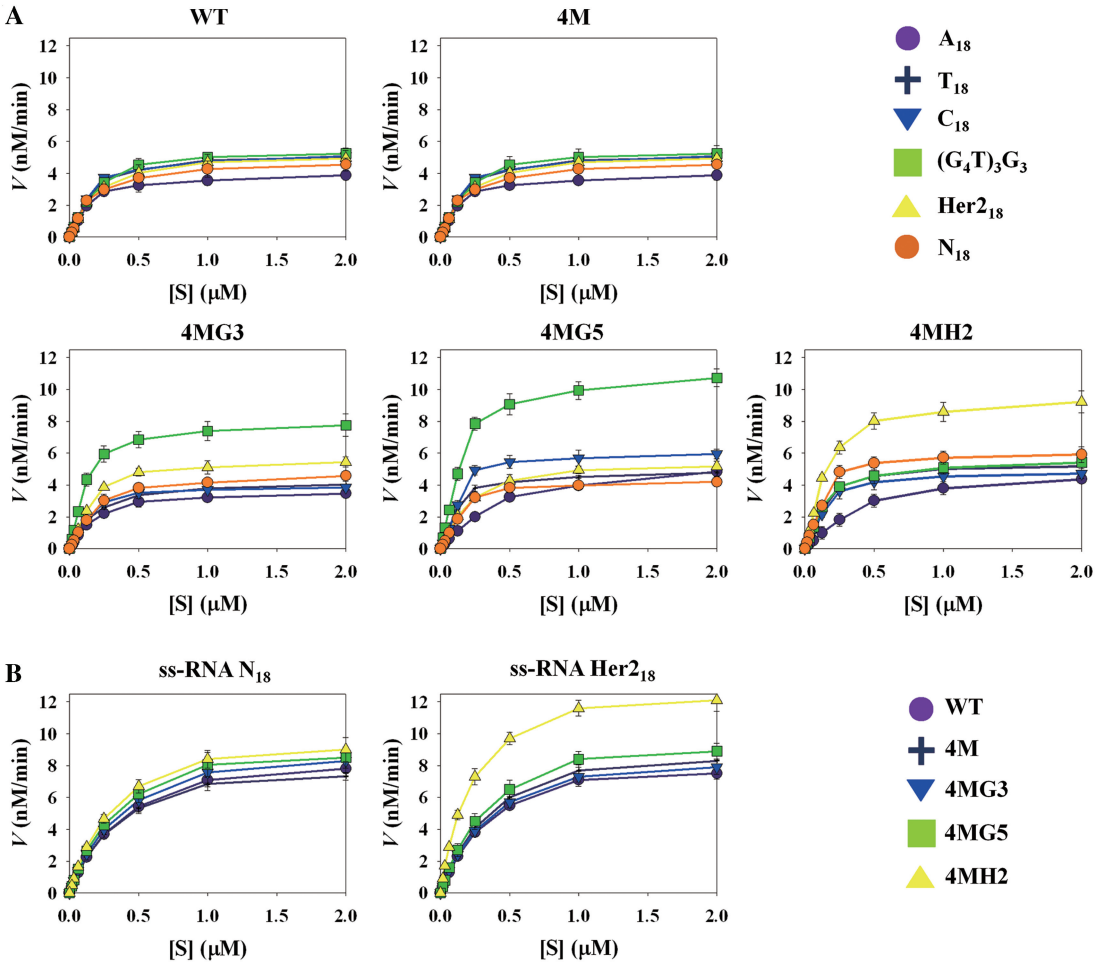

Figure 3. Sequence-specific ss-DNA/RNA hydrolyzing assay of 3D8 VL variants selected against ss-DNA G_{18} (4MG3 and 4MG5) and $Her2_{18}$ (4MH2), compared with 3D8 VL WT and 4M. (A and B) Substrate-concentration dependent initial hydrolyzing velocity (V) of 3D8 VLs were plotted against various 18-bp ss-DNA substrate (S) concentrations (**A**) or 18-bp ss-RNA substrate (S) concentrations (**B**). Each protein (100 nM) was incubated at 37°C with the indicated substrates (16 nM to 2μM), which were double-labeled with 6-FAM at 5′-terminus and its quencher BHQ-1 at 3′-terminus and real-time ss-DNA/RNA hydrolyzing kinetic data were monitored by the fluorescence intensity increase caused by the 6-FAM release from its quencher BHQ-1 due to the hydrolysis (7,18). Due to the difficulty in synthesizing double-labeled ss-DNA G_{18}. 18-bp ss-DNA substrate of $(G_4T)_3G_3$ was used as the G_{18} substrate. The detailed enzymatic kinetic parameters are shown in Table 2. All data points are represented as mean ± SD of three experiments. Lines through mean values represent a mathematical fit of the data using the Michaelis–Menten equation.

kinetics with respect to increasing substrate concentration, demonstrating that 3D8 VLs act as nucleic-acid-hydrolyzing enzymes with substrate preferences. Lineweaver–Burk plot analyses showed that 3D8 VL WT and 4M exhibited similar hydrolyzing efficiencies ($k_{cat}/K_m \approx 2.1–3.4 \times 10^{-6}\,nM^{-1}\,s^{-1}$) with only slight differences in K_m and k_{cat} for all of the ss-DNA substrates tested (Table 2), confirming their sequence non-specific hydrolyzing activity (12,13). In contrast, 3D8 VL variants hydrolyzed their respective target substrates ~2–5-fold more efficiently ($k_{cat}/K_m \approx 7.1–7.8 \times 10^{-6}\,nM^{-1}\,s^{-1}$) than the off-targets ($k_{cat}/K_m \approx 1.6–4.1 \times 10^{-6}\,nM^{-1}\,s^{-1}$) due to their improved substrate affinity (K_m) and catalytic rates (k_{cat}) (Table 2), demonstrating that they preferentially recognized and degraded target substrates. Thus, we designated 4MG3 and 4MG5 as G_{18}-selective and 4MH2 as $Her2_{18}$-selective 3D8 VL variants. When the sequence-selective hydrolyzing activity of 4MH2 was further evaluated for the substrates with the same sequence in ss-RNA form, 4MH2 exhibited ~2-fold higher hydrolyzing efficiency for the target ss-RNA $Her2_{18}$ ($k_{cat}/K_m \approx 10.0 \times 10^{-6}\,nM^{-1}\,s^{-1}$) than the off-target ss-RNA N_{18} ($k_{cat}/K_m \approx 5.1 \times 10^{-6}\,nM^{-1}\,s^{-1}$) (Table 2 and Figure 3B), like the cases for the ss-DNA $Her2_{18}$. However, the other 3D8 VLs showed indistinguishable catalytic efficiency for both ss-RNA $Her2_{18}$ and N_{18}, indicative of their sequence-nonspecific hydrolyzing activities for even ss-RNAs. The catalytic efficiencies (k_{cat}/K_m) of 3D8 VLs for the ss-RNAs ($Her2_{18}$ and N_{18}) were slightly higher than those for the corresponding ss-DNAs by the marginal improved substrate affinity (K_m) and turnover number (k_{cat}) for the ss-RNAs, most likely due to the difference in metal ion-independent and -dependent catalytic mechanism for ss-RNAs and ss-DNAs, respectively (Figure 2). The K_m values of the 3D8 VL variants

Table 2. Kinetic parameters of 3D8 VLs hydrolyzing activity with various 18-bp ss-DNAs and ss-RNAs, derived from the data given in Figure 3[a]

3D8 VLs	Kinetic parameters	ss-DNA substrates (ss-RNA substrates)[b]					
		A_{18}	T_{18}	C_{18}	$(G_4T)_3G_3$[c]	$Her2_{18}$(ss-RNA)	N_{18}(ss-RNA)
WT	K_m (nM)	644 ± 18	568 ± 14	522 ± 18	543 ± 12	549 ± 13 (421 ± 19)	587 ± 11 (441 ± 17)
	k_{cat} (s^{-1}) ($\times 10^{-3}$)	1.6 ± 0.1	1.8 ± 0.1	1.7 ± 0.1	1.9 ± 0.1	1.7 ± 0.1 (1.8 ± 0.1)	1.7 ± 0.1 (1.7 ± 0.1)
	k_{cat}/K_m ($nM^{-1}\,s^{-1}$) ($\times 10^{-6}$)	2.5 ± 0.4	3.2 ± 0.2	3.3 ± 0.1	3.4 ± 0.2	3.0 ± 0.2 (4.2 ± 0.3)	2.8 ± 0.1 (4.0 ± 0.1)
4M	K_m (nM)	614 ± 16	576 ± 15	597 ± 17	525 ± 13*	584 ± 15 (394 ± 12)	576 ± 10 (404 ± 15)
	k_{cat} (s^{-1}) ($\times 10^{-3}$)	1.3 ± 0.2	1.2 ± 0.1*	1.9 ± 0.1*	1.5 ± 0.1	1.5 ± 0.1 (1.8 ± 0.1)	1.5 ± 0.1 (1.6 ± 0.1)
	k_{cat}/K_m ($nM^{-1}\,s^{-1}$) ($\times 10^{-6}$)	2.1 ± 0.1	2.1 ± 0.1*	3.2 ± 0.2*	2.9 ± 0.1	2.5 ± 0.2 (4.4 ± 0.3)	2.6 ± 0.2 (4.0 ± 0.1)
4MG3	K_m (nM)	684 ± 21	829 ± 14*	512 ± 12	297 ± 11*	507 ± 14 (397 ± 14)	559 ± 10 (427 ± 10)
	k_{cat} (s^{-1}) ($\times 10^{-3}$)	1.5 ± 0.1	1.9 ± 0.1	1.3 ± 0.1	2.1 ± 0.1*	1.7 ± 0.1 (1.8 ± 0.1)	1.6 ± 0.1 (1.9 ± 0.1)
	k_{cat}/K_m ($nM^{-1}\,s^{-1}$) ($\times 10^{-6}$)	2.2 ± 0.1	2.3 ± 0.2*	2.6 ± 0.1	7.1 ± 0.3*	3.3 ± 0.2 (4.6 ± 0.2)	2.8 ± 0.1 (4.5 ± 0.2)
4MG5	K_m (nM)	643 ± 16	493 ± 11	522 ± 13	352 ± 13*	643 ± 12 (422 ± 8.6)	601 ± 14 (415 ± 17)
	k_{cat} (s^{-1}) ($\times 10^{-3}$)	1.4 ± 0.2	1.7 ± 0.1	2.0 ± 0.1	2.8 ± 0.1*	1.7 ± 0.1 (2.1 ± 0.1)	1.5 ± 0.1 (2.0 ± 0.1)
	k_{cat}/K_m ($nM^{-1}\,s^{-1}$) ($\times 10^{-6}$)	2.2 ± 0.3	3.3 ± 0.1	3.8 ± 0.3	7.8 ± 0.2*	2.7 ± 0.1 (4.9 ± 0.2)	2.5 ± 0.2 (4.9 ± 0.2)
4MH2	K_m (nM)	758 ± 14*	558 ± 13	527 ± 11	459 ± 14	300 ± 14* (245 ± 12*)	459 ± 19 (395 ± 7)
	k_{cat} (s^{-1}) ($\times 10^{-3}$)	1.2 ± 0.1*	1.8 ± 0.13	1.6 ± 0.1	1.7 ± 0.2	2.2 ± 0.1* (2.4 ± 0.1*)	1.9 ± 0.1 (2.0 ± 0.1)
	k_{cat}/K_m ($nM^{-1}\,s^{-1}$) ($\times 10^{-6}$)	1.6 ± 0.1*	3.3 ± 0.2	3.0 ± 0.2	3.7 ± 0.3	7.3 ± 0.6* (10.0 ± 0.3*)	4.1 ± 0.2 (5.1 ± 0.4)

[a]Enzyme kinetic parameters were obtained by incubating each protein (100 nM) with various substrate concentrations (16 nM–2 μM) at 37°C, as described in Figure 3. All experiments were performed in triplicate and the results are represented as mean ± SD. Significant difference of each kinetic parameter was determined using two-tailed Student's t-test versus the control N_{18} substrate (*$P < 0.01$).
[b]The values for ss-RNA substrates, $Her2_{18}$ and N_{18}, were presented in the parenthesis.
[c]Due to the difficulty in synthesizing the double labeled ss-DNA G_{18} FRET substrate, ss-DNA $(G_4T)_3G_3$ was used as the G_{18} substrate.

for each substrate were not strictly correlated with the substrate affinity (K_D) obtained by SPR (Table 1), indicating a complicated catalytic mechanism in solution. Compared with endonuclease of RNA-induced silencing complex (RISC) involved in RNAi (25), the K_m and k_{cat} values of 3D8 VL variants were ~10-fold higher and slightly lower, respectively, resulting in overally ~10-fold lower catalytic efficiency for target substrates.

3D8 VLs efficiently internalize into living cells and accumulate in the cytosol

The recently identified ability of 3D8 scFv to penetrate into living cells and accumulate in the cytosol without translocating to the nucleus (7) led us to investigate whether 3D8 VLs act similarly. Indeed, human cervical carcinoma HeLa and breast carcinoma SK-BR-3 living cells treated with 3D8 VLs (WT, 4MG3, 4MG5 and 4MH2) exhibited strong 3D8 VL-specific fluorescence signal, compared with untreated cells (Figure 4A). Confocal fluorescence microscopic analysis revealed that all of 3D8 VL proteins dominantly accumulated in the cytosol with little further trafficking into the nucleus (Figure 4B and Supplementary Figure S5), like 3D8 scFv (7). To our best knowledge, this is the first report of single-domain antibodies with the ability to internalize into living cells.

Soluble heparin substantially blocked the internalization of 3D8 VLs (Figure 4C), indicating that 3D8 VLs interact with negatively charged cell surface proteoglycans prior to internalization, like 3D8 scFv (7). Thus, the cell-penetrating ability of 3D8 VLs seems not to be cell type-specific, like other cell-penetrating anti-DNA antibodies and peptides (6,26). To elucidate the specific internalization mechanism, HeLa cells were pre-treated with the following pharmacological inhibitors prior to the addition of 3D8 VLs to interfere with the three major endocytic pathways: chlorpromazine (CPZ) to inhibit clathrin-dependent endocytosis, methyl-β-cyclodextrin (MβCD) to inhibit caveolae/lipid raft endocytosis, and cytochalasin D (Cyt-D) to inhibit macropinocycosis [please refer to the refs. (7,26) for details]. Flow cytometric analyses revealed that pre-incubation of cells with MβCD (5 mM), but neither with CPZ (10 μg/ml) nor Cyt-D (1 μg/ml), led to

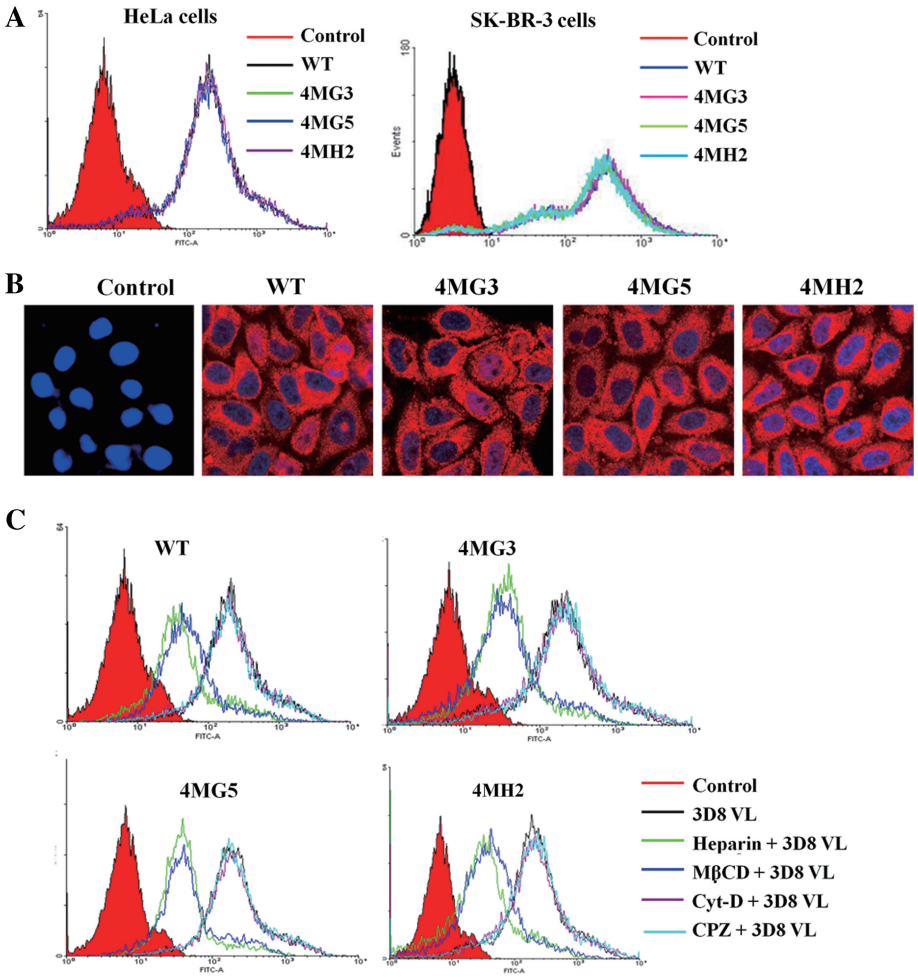

Figure 4. 3D8 VL variants penetrate into living cells by interaction with heparin sulfate proteoglycan on the cell surface and localize dominantly in the cytosol. (**A**) Cellular internalization of 3D8 VLs in HeLa (left panel) and SK-BR-3 (right panel) cells, monitored by flow cytometry. HeLa and SK-BR-3 cells were treated with each 3D8 VL (10 μM) for 2 h at 37°C and then with trypsin to remove surface bound proteins before immunofluorescent labeling of 3D8 VLs with rabbit anti-3D8 polyclonal antibodies and TRITC-labeled anti-rabbit IgG for flow cytometry. (**B**) Internalization and subcellular localization of 3D8 VLs in HeLa cells, untreated ('control') or treated with 10 μM 3D8 VLs at 37°C for 2 h prior to analysis by confocal fluorescence microscopy. 3D8 VLs were stained with rabbit anti-3D8 polyclonal antibodies and TRITC-labeled anti-rabbit IgG (Red). Blue color depicts DAPI-stained nuclei. Centered single confocal sections are shown. Magnification, ×400. (**C**) Effect of pre-treatment of soluble heparin or specific endocytosis inhibitors on the 3D8 VLs cellular uptake, analyzed by flow cytometry. HeLa cells were incubated with 3D8 VLs (10 μM) for 2 h at 37°C with or without pre-treatment of soluble heparin (100 IU/ml), CPZ (10 μg/ml), MβCD (5 mM) and Cyt-D (1 μg/ml) for 30 min prior to flow cytometric analyses.

a significant reduction in the amount of 3D8 VLs internalized (Figure 4C). These results strongly indicated that 3D8 VLs are internalized via caveolae/lipid raft-mediated endocytosis similar to 3D8 scFv (7).

Cell penetrating 3D8 VL variants selectively knockdown target genes

The penetration of 3D8 VLs into living cells and their dominant accumulation in the cytosol prompted us to examine whether 3D8 VLs could selectively degrade mRNAs carrying targeted sequences. When evaluated by EGFP reporter gene with N-terminal G_{18} (G_{18}-EGFP) in HeLa cells, G_{18}-selective 4MG3 and 4MG5 exhibited significant reductions in fluorescence intensity for G_{18}-EGFP but not for intact EGFP (Figure 5A). Semi-quantitative RT-PCRs (20) demonstrated that 4MG3 and 4MG5 selectively decreased only the amount of G_{18}-EGFP mRNA, without significant effects on mRNAs encoding intact EGFP or a house-keeping gene, β-actin (Figure 5B). This result was also reflected at the protein level (Figure 5C). In contrast, 3D8 VL WT did not affect the expression levels of intact EGFP or G_{18}-EGFP.

$Her2_{18}$-selective 4MH2 was incubated with HeLa cells transfected with the full-length Her2 gene. For comparison, a siRNA targeting the same sequence of $Her2_{18}$ in the Her2 gene ($Her2_{18}$-siRNA) was transfected into Her2-transfected HeLa cells. Both 4MH2 and $Her2_{18}$-siRNA, but not 3D8 VL WT, selectively down-regulated Her2 expression at the mRNA and protein levels, without affecting endogenous β-actin expression (Figure 5D and E). Her2 gene silencing by 4MH2 at the mRNA and protein levels was more effective at the earlier time-point of 24 h post-treatment than $Her2_{18}$-siRNA, which exerted substantial Her2 down-regulation after 48 h post-transfection.

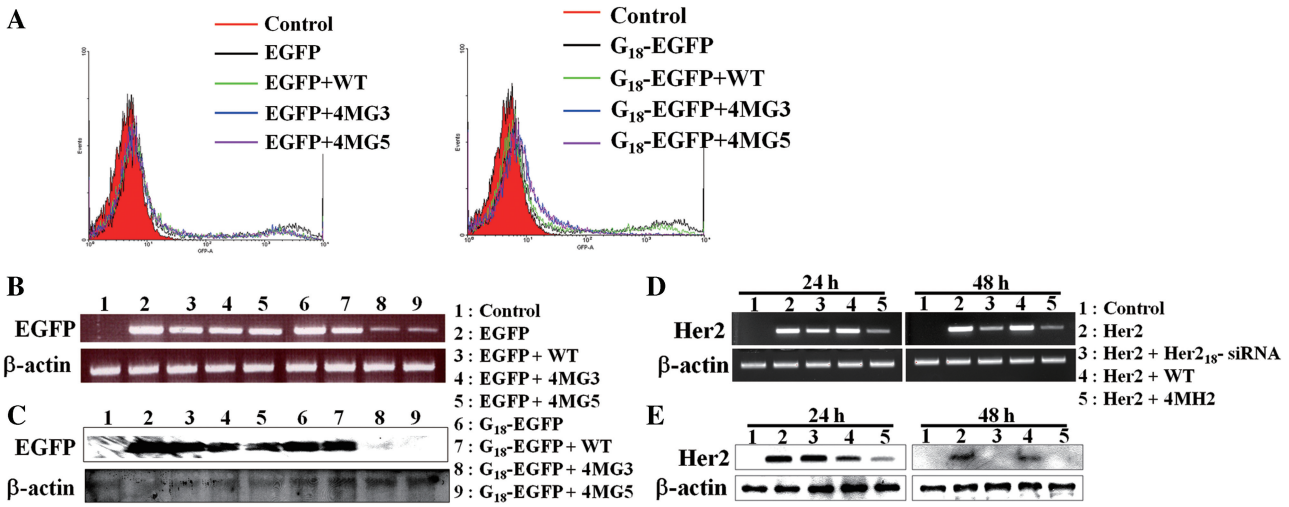

Figure 5. Target gene silencing activity of cell-penetrating 3D8 VL variants in HeLa cells expressing exogenous targeted genes. (A–C) HeLa cells were untransfected ('control') or transfected with plasmids encoding EGFP or G_{18}-EGFP, and 12 h later either untreated or treated at 37°C for 2 h with 3D8 VL WT (10 μM) and G_{18}-selective 4MG3 (10 μM) and 4MG5 (10 μM), and further incubated for 12 h before EGFP expression analyses by flow cytometry (**A**), RT–PCR (**B**) and western blotting (**C**). (D and E) Her2-negative HeLa cells were untransfected ('control') or transfected with a plasmid encoding the full-length Her2 gene, and 24 h later were either untreated or treated at 37°C for 2 h with 3D8 VL WT (10 μM) and $Her2_{18}$-selective 4MH2 (10 μM). After further incubation for 24 or 48 h, Her2 expression was analyzed by RT-PCR (**D**) and western blotting (**E**). After 24 h post-transfection with Her2 gene, HeLa cells were also transfected with $Her2_{18}$-siRNA (500 nM) prior to analyses of Her2 expression at the indicated time. (B–E) Endogenous β-actin served as the protein loading and mRNA abundance control for western blotting and RT-PCR analyses, respectively.

Like the 3D8 VL variants internalized as above, the co-expression of 3D8 VL variants with target sequence-carrying genes in HeLa cells selectively down-regulated the expression levels of targeted proteins by reducing their mRNA levels without significantly affecting off-target genes (Supplementary Figure S6). This result demonstrated that cytosolically expressed 3D8 VL variants also selectively degrade their respective target mRNAs to downregulate the expression of target proteins without significant effects on off-targets.

$Her2_{18}$-selective 4MH2 effectively knocks-down endogenous Her2 expression to induce apoptotic cell death in Her2-overexpressing cells

To determine whether $Her2_{18}$-selective 4MH2 could knockdown the endogenous Her2 transcript by cellular internalization, Her2-overexpressing breast carcinoma SK-BR-3 cells (22) were treated with 4MH2, including other 3D8 VLs for comparisons. 3D8 VL WT and G_{18}-selective 4MG3 and 4MG5 exhibited only slight decreases in Her2 expression after 24 h post-treatment (Figure 6A–C), which was most likely due to non-specific off-target effects. In contrast, 4MH2 greatly reduced the cell surface expression and mRNA levels of Her2 starting 2 h post-treatment, completely abolishing Her2 mRNA detection by 24 h, with only a slight reduction in the mRNA level of off-target β-actin at 48 h (Figure 6A–C). Compared with 4MH2, $Her2_{18}$-siRNA-mediated gene silencing of Her2 was slower and less efficient, decreasing the cell surface expression and mRNA levels after 24 h post-transfection.

While elevated Her2 expression correlates with malignant potential and poor prognosis of several types of carcinomas, silencing of Her2 by siRNA (22,23) or its neutralization by intracellular antibody (intrabody) (27) resulted in growth inhibition and cell death in Her2-overexpressing tumor cells, including SK-BR-3 cells. To investigate whether 4MH2-mediated Her2 gene silencing can exert the similar activity, we treated Her2-overexpressing SK-BR-3 and MDA-MB-231 cells with $Her2_{18}$-selective 4MH2 and then monitored for the cell death, including Her2-negative HeLa cells (27) as a control. 4MH2 treatment significantly induced cell death which was proportional to the post-treatment period in SK-BR-3 (~75% after 48 h) and MDA-MB-231 (~65% after 72 h), but which was moderate in HeLa cells (~30% after 72 h) (Figure 7A). Transfected $Her2_{18}$-siRNA also induced cell death in Her2-overexpressing cells without significant cytotoxicity to HeLa cells. However, Her_{18}-siRNA-mediated cell death of Her2-overexpressing cells was less efficient than 4MH2 during the same period, which is consistent with the relative knockdown efficiency of Her2 (Figure 6).

To elucidate whether apoptosis is the principle mechanism of 4MH2-mediated cell death, cells exposed to 4MH2 were labeled by dual staining of Annexin-V-FITC and propidium iodide (PI) and then analyzed by flow cytometry (19). SK-BR-3 and MDA-MB-231 cells treated with 4MH2 were significantly labeled as early apoptotic cells by Annexin-V-FITC positive staining (Figure 7B), similar to $Her2_{18}$-siRNA, suggesting that 4MH2 induced apoptotic cell death in the Her2-overexpressing cells. 3D8 VL WT and G_{18}-selective 4MG3 and 4MG5 caused ~30–40% cell death after 72 h post-treatment, regardless of the Her2 cellular expression level, demonstrating that 3D8 VLs caused some cytotoxicity, which was probably due to non-specific cellular RNA hydrolysis (7). However, differences in the

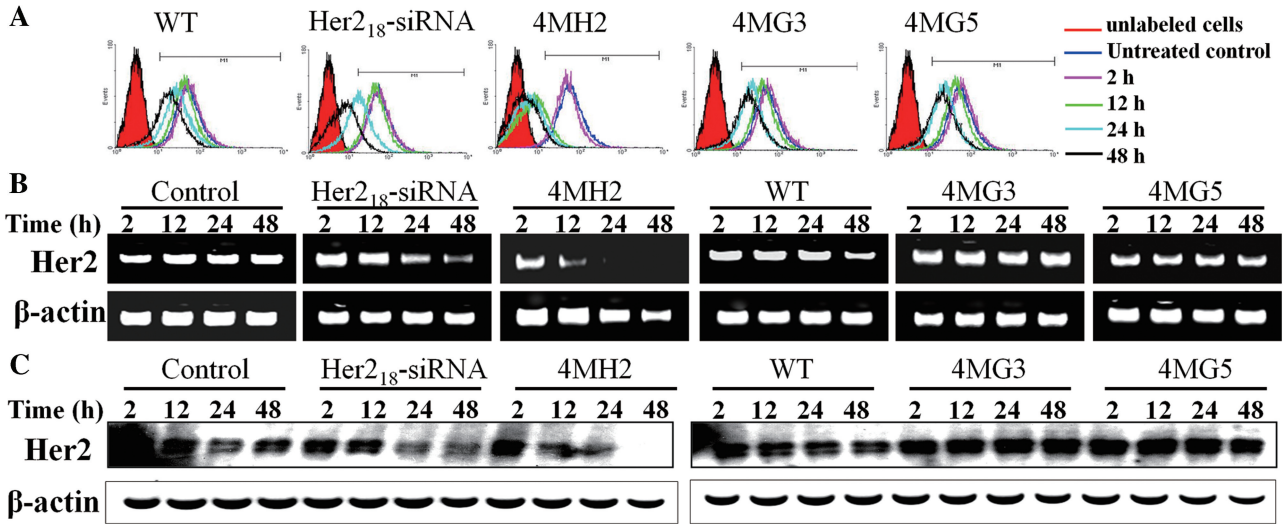

Figure 6. Cell-penetrating Her2$_{18}$-selective 4MH2 knocks-down endogenous Her2 expression in Her2-overexpressing SK-BR-3 cells. SK-BR-3 cells were untreated ('control') or treated with 3D8 VLs (10 μM) for 2 h at 37°C, or transfected with Her2$_{18}$-siRNA (500 nM). Her2 expression was monitored at the cell-surface by flow cytometry (**A**), at the mRNA level by RT-PCR (**B**) and at the protein level by western blotting (**C**) at indicated periods of post-treatment with 3D8 VLs or post-transfection with Her2$_{18}$-siRNA (500 nM). Endogenous β-actin served as the protein loading and mRNA abundance control for western blotting and RT-PCR analyses, respectively. 'Control' indicates untreated cells.

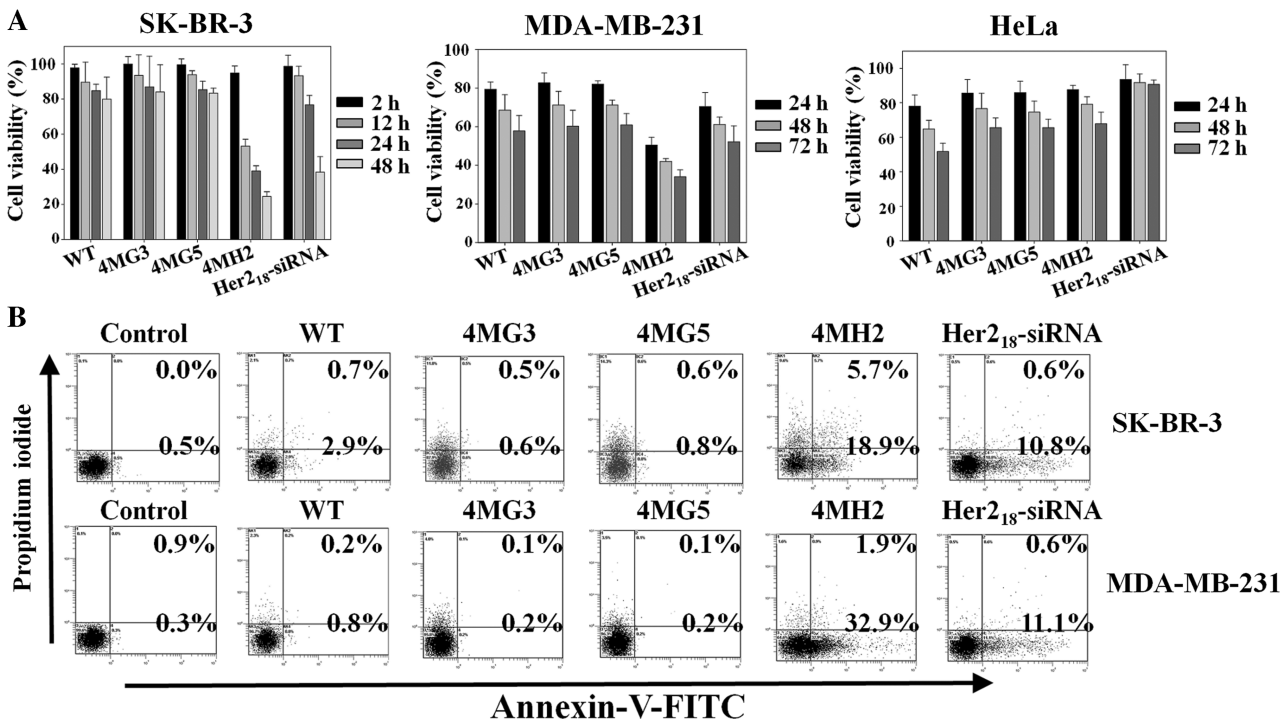

Figure 7. Cell-penetrating Her2$_{18}$-selective 4MH2 induces apoptotic cell death of Her2-overexpressing cells. (**A**) Cell viability assay of Her2-overexpressing SK-BR-3 and MDA-MB-231 cells and Her2-negative HeLa cells at the indicated periods of post-treatment with 3D8 VLs (10 μM) for 2 h at 37°C or post-transfection of Her2$_{18}$-siRNA (500 nM), as monitored by the MTT assay. Percent cell viability was calculated with respect to the untreated control cells. (**B**) Flow cytometry analysis of Annexin-V-FITC and PI staining of Her2-overexpressing SK-BR-3 and MDA-MB-231 cells at 12 h post-treatment with medium only ('control') or with 3D8 VLs (10 μM) for 2 h at 37°C, or at 12 h post-transfection with Her2$_{18}$-siRNA (500 nM). In the dot plots, Annexin-V-FITC$^+$/PI$^-$ cells (lower right quadrant, % shown) and Annexin-V-FITC$^+$/PI$^+$ cells (upper right quadrant, % shown) are considered as 'early apoptotic' and 'dead' cells, respectively.

cell death exerted by 4MH2 (~75%) and other 3D8 VLs (~30–40%) in Her2-overexpressing cells could be attributed the apoptotic cell death induced by the Her2 gene-silencing effects of 4MH2.

DISCUSSION

Antibodies that normally lack the ability to penetrate into living cells have been therapeutically used as targeting proteins, including mainly soluble or cell-surface

expressed antigens (15,19,28). The targeting of intracellular proteins has been achieved by intrabodies (11,28,29). However, intrabodies have never been exploited to knockdown specific proteins at the post-transcriptional mRNA level. Here, we have developed target sequence-selective, hydrolyzing, single-domain antibodies of 3D8 VL variants that can penetrate into living cells and accumulate mostly in the cytosol. These cell-penetrating antibodies (transbodies) recognize and degrade targeted mRNAs, but not proteins, resulting in targeted gene silencing.

We engineered *in vitro* the sequence non-specific DNA/RNA-hydrolyzing 3D8 VL, which has the typical immunoglobulin fold of β-sandwich, into target sequence-selective hydrolyzing variants by randomizing one-sided β-sheet residues. *In vitro* engineering of anti-DNA/RNA antibodies that specifically recognize and hydrolyze specific DNA/RNA antigens has never been reported, although an RNA-binding Fab has been engineered to specifically recognize the targeted RNA tertiary structure (30) and sequence-specific DNA binding antibodies have been raised *in vivo* from mice (31,32). Our results suggest that proteins with β-sheet structure can be used as a scaffold to engineer sequence-specific ss-DNA/RNA binding proteins, as α-helical zinc-finger protein does in specific-specific ds-DNA-binding proteins (33). However, random mutations introduced into the highly conserved framework regions of 3D8 VL, which are otherwise buried in VH–VL interface in IgG format, might induce immunogenic response *in vivo*.

Even though the 18-bp ss-DNAs were employed as screening substrates rather than ss-RNAs due to the higher nucleolytic stability, the selected 3D8 VL variants showed very similar sequence-selective binding and hydrolyzing activities for the targeted sequences in ss-RNA form to those in ss-DNA form *in vitro* (Table 1 and 2), resulting in the preferential hydrolysis of mRNAs carrying the target sequences in the cytosol of cells. In DNA/RNA–protein interactions, stacking and electrostatic interactions play a key role in providing affinity, whereas hydrogen bonds between nucleobase and amino acids dominantly contribute to the sequence-specificity as well as affinity (34). The rank orders of nucleobase–amino acid type correlations have shown strong similarities between the DNA and RNA cases (34,35), suggesting the minor differences between ss-DNA and ss-RNA, including thymine (5-methyluracil) and deoxyribose in DNA in place of uracil and ribose in RNA, do not significantly affect the sequence specificity. Thus, the similar preferential recognition of 3D8 VL variants to their target sequences in either ss-DNA or ss-RNA form suggests that hydrogen bonds between nucleobase and amino acids mainly contribute to their sequence-specificity.

No common patterns of amino acid substitutions were observed among 3D8 VL variants isolated against the same substrates, G_{18} and $Her2_{18}$ (Supplementary Figure S3), suggesting that substituted residues at each position may be involved in more subtle, context-dependent interactions with the target sequences, like the zinc finger-DNA recognition (33). While random mutations without bias to particular amino acids at the targeted residues were observed in the initial library, most of substitutions in the selected 3D8 VL variants occurred with hydrophilic residues (Arg, Asn, Gln, Glu, Ser, Lys, Asp and His), which could readily contribute to base-specific recognition by hydrogen bonds (34). Particularly, the selected 3D8 VL variants showed strong preference for Arg substitution at many residues facing outward, particularly for G_{18}-selective 3D8 VL variants (Supplementary Figure S3). Arg is the most common amino acid interacting with guanine base, the pair of which can form up to four hydrogen bonds, in the analysis of amino acid-base contacts in protein–RNA complexes (34,35). Detailed analysis of the contribution of each substitution to the preferential interaction with target sequences should be waited until the complex structures of 3D8 VL variants with target substrates are obtained.

Many anti-DNA/RNA hydrolyzing antibodies, preferentially found in humans and mice with autoimmune diseases, have been reported to have the ability to penetrate into living cells (6,36–39). Though detailed structural and mechanistic bases how they can cross the plasma membrane of cells remain to be resolved, many studies have suggested that their common feature of possessing a large number of positively-charged amino acids, such as Arg and Lys, in the complementarity-determining regions (CDRs) of VH and/or VL domains due to their antigen binding properties, can be attributed to their internalizing capacity (6,36–39). Thus, like cell-penetrating peptides, non-specific electrostatic interactions of anti-DNA/RNA antibodies with negatively charged cell surface matrix, such as heparan sulfate proteoglycans, have been proposed to contribute to their cell-penetrating activity without cell-type specificity (40,41). 3D8 VL WT and its variants efficiently internalized into the cytosol of living cells most likely by the caveolae/lipid raft-mediated endocytic pathway (Figure 4), like 3D8 scFv (7). Three-dimensional structural analysis of 3D8 VL (17) reveals a continuous patch clustered with positively-charged amino acids composed of Arg27f, Arg29 and Lys30 in CDR1, which is also conserved in the selected 3D8 VL variants (Supplementary Figure S3). This unusual cationic property of 3D8 VLs might explain their cellular internalization capacity, like other cell-penetrating anti-DNA/RNA antibodies (37–41).

Cytoplasmic accumulation of cellular internalized 3D8 VL variants makes it possible to induce gene silencing of targeted genes, like RNAi-mediated gene silencing that primarily occurs in the cytosol (1–3). The knockdown efficiencies of the 3D8 VL variants ranged from 10–100% and increased with the post-treatment period. These ranges are similar to those achieved by conventional siRNA techniques (1–3). $Her2_{18}$-selective 4MH2 induced apoptotic cell death for Her2-overexpressing tumor cells by down-regulating Her2 expression (Figure 6 and 7), indicating that it may have potential as an anti-cancer agent. Compared with $Her2_{18}$-siRNA, the extent to which 4MH2 could knock-down Her2 over a short period (~2 h) of post-treatment (Figure 6), both at the mRNA and protein level, was remarkable. 3D8 VLs in HeLa and SK-BR-3 cells were diffused throughout the

cytosol within ~2 h of medium treatment, with little accumulation in the nucleus, similar to 3D8 scFv (7). The efficient gene silencing effects achieved immediately after cellular internalization of 3D8 VLs distinguishes 3D8 VLs from siRNAs which require at least 12–18 h for effective gene silencing (1–3).

3D8 VL variants exerted significant cytotoxicity (~30–40% after 72 h) compared with siRNA (< 10% after 72 h). The selected 3D8 VL variants showed moderate binding affinities of $K_D \approx 10^{-7}$–10^{-8} M with the target substrates and only ~2–5-fold greater selective hydrolyzing activities for the target sequences than off-targets (Table 1 and 2), which is rather low target specificity compared with other RNA–protein specific interactions (30,34,35). Structural features and molecular docking analysis revealed that 3D8 VLs may interact with only ~5–7 bases of ss-RNA. This suggests that the limited target sequence recognition caused non-specific degradation of other cytosolic RNAs (7), resulting in more cytotoxicity than the 19-bp-targeting siRNA. To minimize off-target effects, modular units of 3D8 VL variants could be linked to confer higher specificity and affinity for long RNA sequences of up to 12–18 bp, as has previously been done for zinc-finger proteins (33).

Interfering transbody-mediated gene silencing may offer several advantages over conventional nucleic-acid based approaches (1–4,10,11), including cell-penetrating ability without the need for exogenous carriers, RNA degradation without external RNases, no nuclease susceptibility, and immediate gene-silencing effects after cellular internalization. These distinct features make interfering transbody an attractive alternative to nucleic-based approaches for modulating gene expression in functional genomics or in therapeutic approaches to diseases such as cancer and viral infections. However, many issues must be addressed to make interfering transbody a more practical and powerful gene-silencing tool for *in vivo* applications, including decreasing the off-target effects and conferring cell- or tissue-specific penetrating abilities.

SUPPLEMENTARY DATA

Supplementary Data are available at NAR Online.

FUNDING

BioGreen 21 Program (20070401034007 and 200807010 34001) from the Rural Development Administration and Priority Research Centers Program from the National Research Foundation (2009-0093826) of the Ministry of Education, Science and Technology, Republic of Korea. Funding for open access charge: The BioGreen 21 Program (20070401034007 and 20080701034001) from the Rural Development Administration and Priority Research Centers, Republic of Korea.

Conflict of interest statement. None declared.

REFERENCES

1. Scherer,L.J. and Rossi,J.J. (2003) Approaches for the sequence-specific knockdown of mRNA. *Nat. Biotechnol.*, **21**, 1457–1465.
2. Tafech,A., Bassett,T., Sparanese,D. and Lee,C.H. (2006) Destroying RNA as a therapeutic approach. *Curr. Med. Chem.*, **13**, 863–881.
3. Carthew,R.W. and Sontheimer,E.J. (2009) Origins and Mechanisms of miRNAs and siRNAs. *Cell*, **136**, 642–655.
4. Cullen,B.R. (2006) Enhancing and confirming the specificity of RNAi experiments. *Nat. Methods*, **3**, 677–681.
5. Makarov,A.A. and Ilinskaya,O.N. (2003) Cytotoxic ribonucleases: molecular weapons and their targets. *FEBS Lett.*, **540**, 15–20.
6. Avrameas,A., Ternynck,T., Nato,F., Buttin,G. and Avrameas,S. (1998) Polyreactive anti-DNA monoclonal antibodies and a derived peptide as vectors for the intracytoplasmic and intranuclear translocation of macromolecules. *Proc. Natl Acad. Sci. USA*, **95**, 5601–5606.
7. Jang,J.Y., Jeong,J.G., Jun,H.R., Lee,S.C., Kim,J.S., Kim,Y.S. and Kwon,M.H. (2009) A nucleic acid-hydrolyzing antibody penetrates into cells via caveolae-mediated endocytosis, localizes in the cytosol and exhibits cytotoxicity. *Cell Mol. Life Sci.*, **66**, 1985–1997.
8. Dow-Tien,C., Yuan-Jhih,T. and Alan,L. (2008) Creating a ribonuclease T-tat that preferentially recognizes and hydrolyzes HIV-1 TAR RNA in vitro and in vivo. *Nucleic Acids Res.*, **36**, 963–969.
9. Melekhovets,Y.F. and Joshi,S. (1996) Fusion with an RNA binding domain to confer target RNA specificity to an RNase: design and engineering of Tat-RNase H that specifically recognizes and cleaves HIV-1 RNA in vitro. *Nucleic Acids Res.*, **24**, 1908–1912.
10. Heng,B.C. and Cao,T. (2005) Making cell-permeable antibodies (Transbody) through fusion of protein transduction domains (PTD) with single chain variable fragment (scFv) antibodies: potential advantages over antibodies expressed within the intracellular environment (Intrabody). *Med. Hypotheses*, **64**, 1105–1108.
11. Muller,S., Zhao,Y., Brown,T.L., Morgan,A.C. and Kohler,H. (2005) TransMabs: cell-penetrating antibodies, the next generation. *Expert Opin. Biol. Ther.*, **5**, 237–241.
12. Kim,D.S., Lee,S.H., Kim,J.S., Lee,S.C., Kwon,M.H. and Kim,Y.S. (2009) Generation of humanized anti-DNA hydrolyzing catalytic antibodies by complementarity determining region grafting. *Biochem. Biophys. Res. Commun.*, **379**, 314–318.
13. Kim,Y.R., Kim,J.S., Lee,S.H., Lee,W.R., Sohn,J.N., Chung,Y.C., Shim,H.K., Lee,S.C., Kwon,M.H. and Kim,Y.S. (2006) Heavy and light chain variable single domains of an anti-DNA binding antibody hydrolyze both double- and single-stranded DNAs without sequence specificity. *J. Biol. Chem.*, **281**, 15287–15295.
14. Lee,H.W., Lee,S.H., Park,K.J., Kim,J.S., Kwon,M.H. and Kim,Y.S. (2006) Construction and characterization of a pseudo-immune human antibody library using yeast surface display. *Biochem. Biophys. Res. Commun.*, **346**, 896–903.
15. Park,K.J., Lee,S.H., Kim,T.I., Lee,H.W., Lee,C.H., Kim,E.H., Jang,J.Y., Choi,K.S., Kwon,M.H. and Kim,Y.S. (2007) A human scFv antibody against TRAIL receptor 2 induces autophagic cell death in both TRAIL-sensitive and TRAIL-resistant cancer cells. *Cancer Res.*, **67**, 7327–7334.
16. Lee,S.H., Carpenter,J.F., Chang,B.S., Randolph,T.W. and Kim,Y.S. (2006) Effects of solutes on solubilization and refolding of proteins from inclusion bodies with high hydrostatic pressure. *Protein Sci.*, **15**, 304–313.
17. Park,S.Y., Lee,W.R., Lee,S.C., Kwon,M.H., Kim,Y.S. and Kim,J.S. (2008) Crystal structure of single-domain VL of an anti-DNA binding antibody 3D8 scFv and its active site revealed by complex structures of a small molecule and metals. *Proteins*, **71**, 2091–2096.
18. Townsend,H.L., Jha,B.K., Han,J.Q., Maluf,N.K., Silverman,R.H. and Barton,D.J. (2008) A viral RNA competitively inhibits the antiviral endoribonuclease domain of RNase L. *RNA*, **14**, 1026–1036.
19. Sung,E.S., Park,K.J., Lee,S.H., Jang,Y.S., Park,S.K., Park,Y.H., Kwag,W.J., Kwon,M.H. and Kim,Y.S. (2009) A novel agonistic

antibody to human death receptor 4 induces apoptotic cell death in various tumor cells without cytotoxicity in hepatocytes. *Mol. Cancer Ther.*, **8**, 2276–2285.
20. Guenin,S., Mauriat,M., Pelloux,J., Van Wuytswinkel,O., Bellini,C. and Gutierrez,L. (2009) Normalization of qRT-PCR data: the necessity of adopting a systematic, experimental conditions-specific, validation of references. *J. Exp. Bot.*, **60**, 487–493.
21. Hackel,B.J., Kapila,A. and Wittrup,K.D. (2008) Picomolar affinity fibronectin domains engineered utilizing loop length diversity, recursive mutagenesis, and loop shuffling. *J. Mol. Biol.*, **381**, 1238–1252.
22. Faltus,T., Yuan,J., Zimmer,B., Kramer,A., Loibl,S., Kaufmann,M. and Strebhardt,K. (2004) Silencing of the HER2/neu gene by siRNA inhibits proliferation and induces apoptosis in HER2/neu-overexpressing breast cancer cells. *Neoplasia*, **6**, 786–795.
23. Choudhury,A., Charo,J., Parapuram,S.K., Hunt,R.C., Hunt,D.M., Seliger,B. and Kiessling,R. (2004) Small interfering RNA (siRNA) inhibits the expression of the Her2/neu gene, upregulates HLA class I and induces apoptosis of Her2/neu positive tumor cell lines. *Int. J. Cancer*, **108**, 71–77.
24. Blackburn,P., Wilson,G. and Moore,S. (1977) Ribonuclease inhibitor from human placenta. Purification and properties. *J. Biol. Chem.*, **252**, 5904–5910.
25. Rana,T.M. (2007) Illuminating the silence: understanding the structure and function of small RNAs. *Nat. Rev. Mol. Cell Biol.*, **8**, 23–36.
26. Duchardt,F., Fotin-Mleczek,M., Schwarz,H., Fischer,R. and Brock,R. (2007) A comprehensive model for the cellular uptake of cationic cell-penetrating peptides. *Traffic*, **8**, 848–866.
27. Wang,T., Zhao,J., Ren,J.L., Zhang,L., Wen,W.H., Zhang,R., Qin,W.W., Jia,L.T., Yao,L.B., Zhang,Y.Q. *et al.* (2007) Recombinant immunoproapoptotic proteins with furin site can translocate and kill HER2-positive cancer cells. *Cancer Res.*, **67**, 11830–11839.
28. Manikandan,J., Pushparaj,P.N. and Melendez,A.J. (2007) Protein i: interference at protein level by intrabodies. *Front Biosci.*, **12**, 1344–1352.
29. Tanaka,T., Williams,R.L. and Rabbitts,T.H. (2007) Tumour prevention by a single antibody domain targeting the interaction of signal transduction proteins with RAS. *Embo J.*, **26**, 3250–3259.
30. Ye,J.D., Tereshko,V., Frederiksen,J.K., Koide,A., Fellouse,F.A., Sidhu,S.S., Koide,S., Kossiakoff,A.A. and Piccirilli,J.A. (2008) Synthetic antibodies for specific recognition and crystallization of structured RNA. *Proc. Natl Acad. Sci. USA*, **105**, 82–87.
31. Bobeck,M.J., Rueda,D., Walter,N.G. and Glick,G.D. (2007) Structural modeling of sequence specificity by an autoantibody against single-stranded DNA. *Biochemistry*, **46**, 6753–6765.
32. Cerutti,M.L., Centeno,J.M., Goldbaum,F.A. and de Prat-Gay,G. (2001) Generation of sequence-specific, high affinity anti-DNA antibodies. *J. Biol. Chem.*, **276**, 12769–12773.
33. Mandell,J.G. and Barbas,C.F. 3rd. (2006) Zinc Finger Tools: custom DNA-binding domains for transcription factors and nucleases. *Nucleic Acids Res.*, **34**, W516–W523.
34. Auweter,S.D., Oberstrass,F.C. and Allain,F.H. (2006) Sequence-specific binding of single-stranded RNA: is there a code for recognition? *Nucleic Acids Res.*, **34**, 4943–4959.
35. Lustig,B., Arora,S. and Jernigan,R.L. (1997) RNA base-amino acid interaction strengths derived from structures and sequences. *Nucleic Acids Res.*, **25**, 2562–2565.
36. Yanase,K. and Madaio,M.P. (2005) Nuclear localizing anti-DNA antibodies enter cells via caveoli and modulate expression of caveolin and p53. *J. Autoimmun.*, **24**, 145–151.
37. Kozyr,A.V., Sashchenko,L.P., Kolesnikov,A.V., Zelenova,N.A., Khaidukov,S.V., Ignatova,A.N., Bobik,T.V., Gabibov,A.G., Alekberova,Z.S., Suchkov,S.V. *et al.* (2002) Anti-DNA autoantibodies reveal toxicity to tumor cell lines. *Immunol. Lett.*, **80**, 41–47.
38. Rivadeneyra-Espinoza,L. and Ruiz-Arguelles,A. (2006) Cell-penetrating anti-native DNA antibodies trigger apoptosis through both the neglect and programmed pathways. *J. Autoimmun.*, **26**, 52–56.
39. Ruiz-Arguelles,A., Rivadeneyra-Espinoza,L. and Alarcon-Segovia,D. (2003) Antibody penetration into living cells: pathogenic, preventive and immuno-therapeutic implications. *Curr. Pharm. Des.*, **9**, 1881–1887.
40. Avrameas,A., Gasmi,L. and Buttin,G. (2001) DNA and heparin alter the internalization process of anti-DNA monoclonal antibodies according to patterns typical of both the charged molecule and the antibody. *J. Autoimmun.*, **16**, 383–391.
41. Zack,D.J., Stempniak,M., Wong,A.L., Taylor,C. and Weisbart,R.H. (1996) Mechanisms of cellular penetration and nuclear localization of an anti-double strand DNA autoantibody. *J. Immunol.*, **157**, 2082–2088.